A hybrid photoelectrocatalytic/photoelectro-Fenton treatment of Indigo Carmine in acidic aqueous solution using TiO_2 nanotube arrays as photoanode

Roger Oriol[a], Ignasi Sirés[a,*], Enric Brillas[a], Adalgisa Rodrigues De Andrade[b,c**]

[a] *Laboratori d'Electroquímica dels Materials i del Medi Ambient, Departament de Química Física, Facultat de Química, Universitat de Barcelona, Martí i Franquès 1-11, 08028 Barcelona, Spain*

[b] *Departamento de Química, Faculdade de Filosofia, Ciências e Letras de Ribeirão Preto, Universidade de São Paulo, 14040-901, Ribeirão Preto, SP, Brazil*

[c] *National Institute for Alternative Technologies of Detection, Toxicological Evaluation and Removal of Micropollutants and Radioactives (INCT-DATREM), UNESP, Institute of Chemistry, P.O. Box 355, 14800-900, Araraquara (SP), Brazil*

Paper submitted for publication in the *Journal of Electroanalytical Chemistry*

Corresponding author: * E-mail: i.sires@ub.edu (I. Sirés)

** E-mail: ardandra@ffclrp.usp.br (A.R. De Andrade)

Abstract

This article reports the synthesis of TiO_2 nanotube arrays (TiO_2 NTs), grown by Ti anodization, and their use as photoanode in a hybrid photelectrocatalytic (PEC)/photoelectro-Fenton (PEF) treatment of Indigo Carmine solutions in sulfate medium at pH 3.0. The anode was combined with an air-diffusion cathode that ensured continuous H_2O_2 electrogeneration. Comparative trials by electrochemical oxidation with electrogenerated H_2O_2 (EO-H_2O_2), electro-Fenton (EF) and PEF with Pt anode were made. The photoanode was stable operating up to 3 mA cm^{-2} with irradiation from a 36-W UV LED lamp, showing photoelectroactivity from an anodic potential (E_{an}) of +0.20 V, as determined by cyclic voltammetry. At 3 mA cm^{-2}, color removal by EO-H_2O_2 with Pt and PEC with TiO_2 NTs was very slow, being much faster in EF, PEF and PEC/PEF due to main role of $^{\bullet}OH$ formed from Fenton's reaction upon addition of Fe^{2+}. The absorbance and dye concentration decays agreed with a pseudo-first-order kinetics, yielding a slightly lower rate constant for decolorization because of the formation of colored products. The mineralization ability increased as: EO-H_2O_2 << EF << PEF < PEC/PEF. The holes photogenerated at the TiO_2 NTs surface had higher oxidation ability than $^{\bullet}OH$ formed at the Pt surface from water discharge. In PEC/PEF, a slower mineralization was found at 2 mA cm^{-2}, although the final mineralization percentage was similar to that attained at 3 mA cm^{-2}. Both, SO_4^{2-} and NH_4^+ ions were released during the treatments, along with isatin-5-sulfonic and formic acids as main products.

Keywords: Indigo Carmine; Photoelectrocatalysis: Photoelectro-Fenton; Anodized Ti; Water treatment

1. Introduction

Societal development requires more stringent environmental policies, which in turn demand more effective and efficient technologies for the remediation of natural water as well as urban and industrial wastewater. Continuous discharge of toxic, non-biodegradable organic pollutants in such matrices is potentially hazardous for humans and animals [1,2]. Since most organic pollutants are not destroyed by conventional methods, it is mandatory to devise more powerful processes. Among them, a wide range of electrochemical advanced oxidation processes (EAOPs) exhibits very appealing features like simplicity, effectiveness, low operation expenses and viability under mild conditions [1-5].

To date, the most successful EAOP is electrochemical oxidation (EO). This method promotes the removal of dissolved organic molecules upon electron flow between a power supply and an anode/cathode pair [1]. Organics can be oxidized either by direct charge transfer at the anode (M) surface or, at high current, by an adsorbed oxidant like hydroxyl radical, denoted as M(•OH), formed as intermediate as a result from the large overpotential that promotes the water discharge to O_2 gas from reaction (1) [1,5,6]:

$$M + H_2O \rightarrow M(^{\bullet}OH) + H^+ + e^- \quad (1)$$

In classical EO, the cathode does not contribute to decontamination since it simply favors H_2 gas evolution from H^+ or H_2O reduction. The use of a carbonaceous cathode fed with O_2 gas or air allows the alternative production of H_2O_2 from reaction (2) [2,3,5]:

$$O_{2(g)} + 2H^+ + 2e^- \rightarrow H_2O_2 \quad (2)$$

H_2O_2 is a reactive oxygen species (ROS) with much smaller oxidation power than •OH, and gives rise to the so-called EO with electrogenerated H_2O_2 (EO-H_2O_2) [2,5]. The oxidation ability of H_2O_2 can be substantially upgraded upon occurrence of Fenton's reaction (3). In the

foundational and simplest version, i.e., electro-Fenton (EF) process, homogeneous •OH is produced in the bulk as the electrogenerated H_2O_2 reacts with a catalytic amount of Fe^{2+} at an optimum pH of 2.8 [2]. Carbon felt [7-9] and gas-diffusion electrodes [10-12] are typically employed cathode materials in this method. The main drawback of EF is the formation of final Fe(III)-carboxylate complexes that are very slowly destroyed by heterogeneous M(•OH) and homogeneous •OH, thus impeding the overall mineralization unless continuous Fe^{2+} regeneration is ensured. Fe(III) reduction is feasible in photoelectro-Fenton (PEF) thanks to photo-Fenton reaction (4) promoted by UVA light irradiating the solution, which also allows the photodecomposition of the refractory complexes, eventually yielding a higher mineralization degree [2,11,13].

$$Fe^{2+} + H_2O_2 \rightarrow Fe^{3+} + {}^{\bullet}OH + OH^- \quad (3)$$

$$[Fe(OH)]^{2+} + h\nu \rightarrow Fe^{2+} + {}^{\bullet}OH \quad (4)$$

The degradation power of the above EAOPs is highly dependent on the anode nature and its ability to produce M(•OH) from reaction (1) [1,5,6,11]. In sulfate medium, the non-active boron-doped diamond (BDD) anode is needed in EO, EO-H_2O_2 and EF with an air-diffusion cathode, because BDD(•OH) is more effective for organic matter removal than M(•OH) formed on active anodes like Pt or IrO_2 [5,14]. In PEF, however, the results are quite similar with both types of anodes because the powerful photolytic action of UVA photons over the reaction by-products is the main contribution to mineralization.

Another type of EAOP is photoelectrocatalysis (PEC), based on the illumination of a semiconductor that acts as photoanode in the electrolytic cell [15,16]. The bandgap energy (E_{gap}) must be lower than the energy of incident photons to promote the jump of an electron from the valence band (VB) to the conduction band (CB). This creates two kinds of charge carriers, i.e., an electron in the CB (e^-_{CB}) and a positively charge vacancy or hole in the VB

(h^+_{VB}), according to reaction (5). In the absence of applied current, i.e., photocatalysis process, a fast recombination of the e^-_{CB}/h^+_{VB} pair occurs, which is greatly minimized upon current supply because the cathode acts as a sink for photogenerated e^-_{CB} coming from the photoanode. In PEC, a high amount of heterogeneous P(•OH) can be produced at the photoanode (P) surface from the oxidation of water by h^+_{VB} via reaction (6) [16], largely upgrading the decontamination process.

$$\text{Photoanode} + h\nu\ (\geq E_{gap}) \rightarrow e^-_{CB} + h^+_{VB} \quad (5)$$

$$\text{Photoanode} + h^+_{VB} + H_2O \rightarrow P(^\bullet OH) + H^+ \quad (6)$$

TiO_2, in its crystalline anatase phase, is the most widespread material for photocatalysis and PEC. It is non-toxic, abundant, cheap and its E_{gap} = 3.2 eV [16] ensures a high quantum yield for reaction (5) under UVA irradiation. Recently, TiO_2 nanotubes (TiO_2 NTs) have shown greater effectiveness for the removal of organics, owing to their larger surface area providing more active sites for both, adsorption and carrier generation via reaction (5) [17,18]. Despite this, the PEC process still has low oxidation ability because the photoanode produces a small photocurrent under UVA light irradiation. Several authors have reported a higher performance by combining PEC with EF [19] and PEF with TiO_2 [20], Au-TiO_2 [21], raw TiO_2 NTs [22-24], modified TiO_2 NTs [25,26], or nanometric ZnO instead of TiO_2 [27,28]. However, the comparison between PEF and hybrid PEC/PEF (i.e., PEC and PEF simultaneously performed in the same cell) under analogous conditions has not been addressed in detail so far, despite its particular importance in order to draw sound conclusions for operation at low current.

Indigo Carmine (disodium salt of 3,3'-dioxo-2,2'-bi-indolinylidene-5,5'-disulfonic acid, $C_{16}H_8N_2Na_2O_8S_2$, see molecular structure of its acid form in Fig. 1a) is one of the oldest and most important industrial dyes, being employed to dye clothes and other blue denim [29,30]. This dye is toxic for microorganisms, rats, pigs and humans [31]. Several works have described

the destruction of Indigo Carmine by photocatalysis with TiO_2 [31,32], CdS_2 [33] or $SrZnTiO_3$/g-C_3N_4 [34], PEC with a TiO_2 [35], TiO_2/WO_3 [36] or TiO_2 NTs [37] photoanodes, EO with BDD [29,38], SnO_2-based [39-41], PbO_2 [40], Pt [42] or Ru-doped Pt [43], EF with BDD [30] or Pt [42] and PEF with BDD [30]. Indigo (3,3'-dioxo-2,2'-bi-indolinylidene) and isatin-5-sulfonic acid (1H-Indole-2,3-dione-5-sulfonic acid) have been detected as primary products, whereas oxalic and oxamic acids appeared as final carboxylic acids [29,30,36]. The molecular structures of indigo and isatin-5-sulfonic acid are shown in Fig. 1b and c, respectvely. As far as we are concerned, no previous work addressed the PEC/PEF treatment of Indigo Carmine solutions.

In this work, a TiO_2 NTs photoanode synthesized by Ti anodization has been characterized and used for the PEC/PEF treatment of a 0.260 mM Indigo Carmine solution in sulfate medium at pH 3.0. Note that this Indigo Carmine concentration is typical of dye wastewater. An air-diffusion cathode was used for H_2O_2 production. Comparative experiments were made by EO with a Pt/stainless steel cell as well as by EO-H_2O_2, EF and PEF with a Pt/air-diffusion cell in order to understand the behavior of the TiO_2 NTs photoanode and the viability of the PEC/PEF process. Released inorganic ions, primary products and final carboxylic acids were identified to completely characterize the mineralization process of the dye solutions in PEC/PEF.

2. Experimental

2.1. Chemicals

Reagent grade Indigo Carmine (> 97% purity), isatin 5-sulfonic acid sodium salt dihydrate (> 98% purity) and indigo (95% purity) were purchased from Sigma-Aldrich. Carboxylic acids, Na_2SO_4, $FeSO_4 \cdot 7H_2O$ and concentrated H_2SO_4 (95-97% purity) were of analytical grade purchased from Merck, Fluka, Panreac and Acros Organics, respectively. High-purity water from Millipore Milli-Q (resistivity > 18.2 MΩ cm) was utilized for the preparation of all

aqueous solutions. Other chemicals used for synthesis and analysis were of HPLC or analytical grade purchased from Panreac, Probus and Merck.

2.2. Synthesis of TiO_2 NTs photoanodes

TiO_2 NTs were grown by Ti anodization following the procedure reported by Almeida et al. [19]. To sum up, Ti sheets (2.0 cm × 6.0 cm) from Sigma-Aldrich (99.99% purity) were firstly polished and then consecutively degreased in isopropyl alcohol and ultrapure water for 30 min. Afterwards, they were boiled in a 10% oxalic acid solution for 30 min to ensure that all TiO_2 was removed. Each Ti sheet was introduced as the anode in an electrolytic cell, using a stainless steel mesh as the cathode. A glycerol solution containing 0.25 wt.% NH_4F and 10 vol.% ultrapure water was used as the background electrolyte. A constant potential of 30 V was applied between the electrodes for 50 min. After galvanostatic anodization, the synthesized Ti/TiO_2 NTs sheets were heated at 450 °C for 30 min to convert the amorphous TiO_2 to crystalline anatase phase.

2.3. Electrolytic systems for H_2O_2 generation and Indigo Carmine removal

The electrolytic trials were carried out with two kinds of anodes, namely the synthesized TiO_2 NTs and a Pt sheet (99.99% purity) purchased from SEMPSA (Barcelona, Spain). Both electrodes were covered with PTFE tape, leaving an uncovered area of 3 cm^2 to be further exposed to the solutions. The cathode, with the same exposed area, was either a carbon-PTFE air-diffusion electrode purchased from E-TEK (Somerset, NJ, USA) or a stainless steel (AISI 304) sheet. The electrolytic cell was an open glass tank reactor that contained the two electrodes separated about 1 cm and 150 mL of solution. The mass transport was ensured by vigorous magnetic stirring. The cell was jacketed to maintain the solution temperature at 25 ºC under circulation of thermostated water. The air-diffusion cathode became operative upon air pumping through its inner dry side at a flow rate of 600 mL min^{-1}, yielding a continuous

156 production of H_2O_2 from reaction (2) at its outer wet side. All the trials were made under
157 galvanostatic mode and the constant current density (*j*) was provided by an EG&G Princeton
158 Applied Research 273A potentiostat-galvanostat. A Demestres 601BR digital multimeter was
159 utilized to directly monitor the cell voltage.

160 The PEF experiments with a Pt/air-diffusion cell and the PEC/PEF trials with a TiO_2
161 NTs/air-diffusion cell (a sketch of the cell used in PEC/PEF is shown in Fig. 2.) for the treatment
162 of Indigo Carmine solutions were run in the presence of 0.050 M Na_2SO_4 as supporting
163 electrolyte and 0.50 mM Fe^{2+} as catalyst, after adjustment to pH 3.0 with H_2SO_4 and under
164 solution irradiation with a SUNUV SUN9X 36-W UV LED double light source (λ_{max} = 365 nm
165 and 405 nm), with 29 W m^{-2} irradiance measured at the solution surface. This semicircular lamp
166 surrounded the cell at distance of 2.0-2.5 cm, being placed inside a box made of mirrors to
167 enhance the photon absorption by the photocatalyst. The pH value and Fe^{2+} concentration were
168 chosen on the basis of previous studies on PEF [13,44]. The same conditions, but in the absence
169 of the dye, were employed to determine the accumulated H_2O_2. Comparative assays by EO-
170 H_2O_2 were performed without catalyst and in the dark, using a Pt/air-diffusion cell.

171 *2.4. Analytical procedures*

172 Field emission scanning electron microscopy (FE-SEM) analysis was made with a JEOL
173 JSM7100F. The sample was coated with carbon using a high vacuum Emitech K-950X
174 vaporizer. Elements present in the TiO_2 NTs sheet before and after electrolytic treatments were
175 identified by energy dispersive X-ray (EDX) technique with an Oxford Instruments INCA 200
176 detector coupled to the microscope.

177 Cyclic voltammetry was performed in a conventional three-electrode cell containing 80
178 mL of 0.050 M Na_2SO_4 solution at pH 3.0 and 25 ºC. The working electrode was a synthesized
179 TiO_2 NTs of 1 cm^2 geometric area, the counter electrode was a Pt sheet and the reference
180 electrode was a saturated calomel electrode (SCE). All potentials are referred to SCE. Cyclic

voltammograms were recorded between -2.00 and +3.00 V at a scan rate of 10 mV s^{-1} using a Methrom Autolab PGSTAT30 potentiostat/galvanostat. The experiments were carried out either in the dark or under illumination with the above UV LED lamp. Chronoamperometry was made with the same equipment and consecutive *j-t* plots were obtained at +0.20 V, a potential value at which the photoanode started to produce photocurrent, setting an on/off cycle of 60 s dark/60 s light.

The solution pH was monitored with a Crison GLP 22 pH-meter. The concentration of accumulated H_2O_2 was determined by the titanium sulfate colorimetric method using a Unicam UV/Vis UV4 spectrometer set at λ = 408 nm [45]. Prior to analysis, all the samples were filtered with 0.45 μm PTFE filters from Whatman. Total organic carbon (TOC) determinations of the initial and treated solutions were made with a Shimadzu VCSN TOC analyzer. The non-purgeable organic carbon (NPOC) method was utilized with ±1% reproducibility.

The decolorization of treated solutions was assessed from their absorbance (*A*) decay using the above spectrophotometer. Samples withdrawn were diluted with ultrapure water (1:4 (v/v)) and their *A* value was immediately measured at λ = 611 nm (the maximum wavelength of Indigo Carmine). The concentrations of the dye and its aromatic by-products were monitored by reversed-phase high-performance liquid chromatography (HPLC). Before this, the samples collected from the EF, PEF and PEC/PEF treatments were diluted with the mobile phase (1:1 (v/v)) to stop de degradation process. The analysis was made with a Waters 600 LC coupled to a Waters 996 photodiode array detector. The organic components were separated with a Thermo BDS Hypersil C-18 5 μm (250 mm × 4.6 mm (i.d.)) column at 35 ºC, upon elution with a 70:30 (v/v) 0.05 M phosphate buffer (pH 7.2) + 0.01 M tetrabutylammonium hydrogensulfate/acetonitrile mixture at 0.8 mL min^{-1}. Indigo Carmine and isatin-5-sulfonic acid appeared at retention time (t_r) of 7.2 and 4.9 min, respectively, and were quantified at λ values of 611 and 243 nm. The detection of produced final carboxylic acids was made by ion-exclusion

HPLC, fitting the LC with a Bio-Rad Aminex® HPX-87H (300 mm × 7.8 mm (i.d.)) column at 35 ºC [13]. The chromatograms displayed well-defined peaks related to oxalic (t_r = 6.7 min), oxamic (t_r = 9.3 min) and formic (t_r = 13.9 min) acids. NH_4^+, SO_4^{2-} and NO_3^- concentrations were determined as reported in earlier work [13,46].

All the decolorization and degradation assays were carried out at least in duplicate. Average values of all determined parameters are depicted and figures show the error bars obtained with a 95% confidence interval.

3. Results and discussion

3.1. Physical characterization of TiO_2 NTs

The morphology of the synthesized TiO_2 NTs was studied by FE-SEM analysis. Fig. 3a depicts a general view of a pristine photoanode grown by Ti anodization. It shows a uniform distribution of the nanotubes with some evident cracks, which appear during the last step of the synthesis procedure involving the sintering at 450 ºC to obtain the anatase phase. As shown in Fig. 3b, the surface cracking is much less remarkable after prolonged use of TiO_2 NTs as photoanode in the PEC/PEF treatment of a 0.260 mM Indigo Carmine solution in 0.050 M Na_2SO_4 at pH 3.0 and low j values of 2 and 3 mA cm^{-2} (E_{an} of +5.6 and +6.2 V vs. SCE). This suggests the occurrence of surface modification during the photoelectrochemical assays. In particular, the electrode polarization promoted a greater compaction of the electrode surface, diminishing the number and width of the cracks. Therefore, this stabilized electrode with a more homogeneous surface was the one employed in further degradation trials, in order to ensure a good reproducibility of the results, as will be confirmed below. The size of the prepared TiO_2 NTs was measured, and some inner and outer diameters are collected in Fig. 3c and d, respectively. As can be seen, the inner diameters of nanotubes in the pristine electrode varied between 81 and 111 nm, whereas the values of the outer ones were of 147-168 nm, thus

accounting for a nanometric wall thickness. On the other hand, Fig. 3e depicts the cross-section image, revealing an average thickness of 340 µm for the Ti substrate. The grown nanotubes on top of it can be better observed in Fig. 3f, which shows an estimated average length around 1 µm. All these data reveal that the synthesized photoanodes possessed a large active area that could probably favor the generation of high amounts of P(•OH) from reaction (6) upon UV illumination during the PEC/PEF treatment of the Indigo Carmine solutions.

EDX analysis of the above pristine and used photoanodes was carried out to determine the elements present in their surface. As can be seen in Fig. 4a, only Ti and O were detected for the pristine sheet, thus verifying the appropriateness of the cleaning protocol after the Ti anodization. In contrast, Fig. 4b reveals the presence of small amounts of Na and S in the used electrode, having become adsorbed from the supporting electrolyte, i.e., Na_2SO_4. Traces of C coming from the adsorption of some oxidation product of Indigo Carmine can be observed as well. The good reproducibility obtained for the degradation assays of this dye by PEC/PEF, as will be reported in next subsections, ensures the scarce influence of these impurities on the ability of the photoanode to photogenerate e^-_{CB}/h^+_{VB} pairs via reaction (5) and the subsequent production of P(•OH) via reaction (6).

3.2. Electrochemical characterization of the TiO_2 NTs

Cyclic voltammetry was utilized to characterize the electrochemical behavior of the TiO_2 NTs as photoanode in a 0.050 M Na_2SO_4 solution at pH 3.0 operating either in the dark (EO conditions) or under irradiation with a 36-W UV LED lamp (PEC conditions). Pt was used as counter electrode to avoid the formation of H_2O_2, which might have an effect on the behavior of the anode. Fig. 5a presents a typical cyclic voltammogram recorded between -2.00 and +3.00 V at a scan rate of 10 mV s^{-1}. The same profile was obtained after a series of consecutive cycles, confirming the high stability of the electrode surface. In the dark, an onset potential of +1.70 and -1.30 V for O_2 and H_2 evolutions, respectively, can be observed. In the middle of the

potential range under study, a small oxidation peak with anodic peak potential (E_p^a) of -0.02 V appeared, associated as redox pair with a first small reduction peak with cathodic peak potential (E_p^c) of -0.18 V. At slightly more negative potentials, another small reduction peak at E_p^c = -0.59 V was found before the H_2 discharge. The former pair can be related to the Ti^{IV}/Ti^{III} equilibrium [18], whereas the subsequent irreversible cathodic peak can be ascribed to a charge compensation through the intercalation of protons as follows [47]:

$$Ti^{IV}O_2 + H^+ + e^- \rightarrow Ti^{III}(O)(OH) \quad (7)$$

In Fig. 5a, it can also be observed that the irradiation of the TiO_2 NTs with the UV LED lamp did not modify its electrocatalytic activity regarding the O_2 and H_2 discharges and the Ti^{IV}/Ti^{III} redox process. However, an increase in *j* from 0.08 to 0.63 mA cm^{-2} when the potential was scanned from +0.20 to +1.70 V can be observed. This is due to photocurrent induced upon generation of charge carriers (e^-_{CB} and h^+_{VB}) via reaction (5), which is crucial to undertake successful degradation tests with Indigo Carmine solutions.

To corroborate the photocurrent generation upon light irradiation, a chronoamperometric study was performed using a 0.100 M Na_2SO_4 solution at pH 3.0 and an E_{an} = +0.20 V (i.e., the onset potential that allowed producing the photocurrent) in on/off cycles of 60 s by switching on and off the 36-W UV LED lamp. Fig. 5b illustrates the very low *j* obtained when the lamp was switched off, whereas the *j* value strongly increased up to about 120 μA cm^{-2} when it was switched on, as expected from the flow of photogenerated e^-_{CB}. In the first cycle, a progressive activation of the photoanode with increasing *j* occurred until the maximum value was attained, whereas it was rather reached instantaneously in all subsequent on/off cycles. These findings confirm the large ability of the synthesized TiO_2 NTs to photogenerate the e^-_{CB}/h^+_{VB} pairs, thus producing P($^\bullet$OH) that can be employed for the removal of organic pollutants.

3.3. H_2O_2 production at low current density

279 The H_2O_2 accumulated in a 0.050 M Na_2SO_4 solution at pH 3.0 that was produced at the
280 air-diffusion cathode was assessed by PEF with a Pt anode and PEC/PEF with a TiO_2 NTs
281 photoanode, in the presence of 0.50 mM Fe^{2+} and under illumination of the solution with UV
282 light. As can be seen in Fig. 6a, the H_2O_2 concentration rose gradually in both cases, attaining
283 a steady state value of 2.6 mg L^{-1} in PEF and a slightly higher value of 3.2 mg L^{-1} in PEC/PEF.
284 The H_2O_2 accumulation depended on the relative ratio of its electrogeneration and destruction
285 rates, achieving the maximum contents once both rates became equal [2,5]. This occurs when
286 H_2O_2 originated via reaction (2) is destroyed at the same rate by a combination of several
287 reactions: Fenton's reaction (3), stimulated by the photolytic reaction (4), the attack of
288 homogeneous $^{\bullet}OH$ from reaction (8), and its oxidation at the anode to produce O_2 gas from
289 consecutive reactions (9) and (10). In the two latter cases, the weak oxidant hydroperoxyl
290 radical ($HO_2^{\bullet}$) was formed.

291 $$H_2O_2 + {}^{\bullet}OH \rightarrow HO_2^{\bullet} + H_2O \quad (8)$$

292 $$H_2O_2 \rightarrow HO_2^{\bullet} + H^+ + e^- \quad (9)$$

293 $$HO_2^{\bullet} \rightarrow O_{2(g)} + H^+ + e^- \quad (10)$$

294 The percentage of current efficiency (CE) was calculated considering that the theoretical
295 H_2O_2 electrogeneration obeyed the Faraday's law as follows:

296 $$\mathrm{CE} = \frac{2\,F\,V\,[\mathrm{H_2O_2}]}{I\,t}\,100 \quad (11)$$

297 where 2 is the number of electrons consumed for H_2O_2 generation from reaction (2), F is the
298 Faraday constant, V is the solution volume (in L) and $[H_2O_2]$ is the accumulated H_2O_2
299 concentration (in M) at given current I (in A) and electrolysis time t (in s).

300 Fig. 6b illustrates the progressive decrease of CE as the electrolysis was prolonged in both
301 EAOPs. Maximum values of 107% and 101% in PEF and PEC/PEF, respectively, can be

observed, decreasing down to 34% and 41%. This decay is due to the gradual increase in rate of destruction reactions (3), (4), (8) and (9), thus reducing its accumulation rate. The slightly superior percentage of CE under PEC/PEF conditions as compared to PEF suggests the slower anodic oxidation of H_2O_2 at the TiO_2 NTs photoanode as compared to the Pt anode, since similar rates are expected for bulk reactions (2)-(4) and (8). These findings confirm that the air-diffusion cathode produces a high amount of H_2O_2 in all EAOPs tested, ensuring the generation of homogeneous $^{\bullet}OH$ with ability to destroy the organic pollutants.

3.4. Indigo Carmine removal

A preliminary study was made by adding 5 mM H_2O_2 into a 0.260 mM Indigo Carmine solution containing 0.050 M Na_2SO_4 at pH 3.0. No decolorization was observed, indicating that the dye oxidation by H_2O_2 is insignificant. This means that the degradation of organics in the EAOPs can be accounted for by the action of other oxidants generated in situ. Several decolorization assays with the above solution but in the presence of 0.50 mM Fe^{2+} were performed by PEC/PEF with a synthesized TiO_2 NTs photoanode and an air-diffusion cathode at a constant j up to 10 mA cm^{-2}. Stable conditions were obtained only at $j \leq 3$ mA cm^{-2} and hence, this value was chosen to carry out the comparison with other methods.

Fig. 7a depicts a very slow color removal for the acidic Indigo Carmine solutions under PEC, EO and EO-H_2O_2 conditions, regardless of the electrodes used. After 120 min of electrolysis at j = 3 mA cm^{-2}, 45% removal was achieved using a Pt/stainless steel cell, being higher than 37% found with a Pt/air-diffusion cell. The slow removals can be related to the scarce ability of the Pt anode to destroy organics at such low j value, because of the very small production of oxidant Pt($^{\bullet}OH$) from reaction (1). On the other hand, it is well known that the high selectivity of the air-diffusion cathode to form H_2O_2 hinders other cathodic reactions to great extent [2]. This suggests that the superior decolorization attained with the stainless steel cathode may be due to the reduction of colored organics on its surface. The percentage of color

removal was slightly upgraded when the PEC process with a TiO_2 NTs photoanode and an air-diffusion cathode was run under the same conditions, achieving a value of 46% at 120 min. This means that the irradiated photoanode produces a significant amount of h^+_{VB} from reaction (5), with ability to attack the parent molecule and its colored by-products, either directly or via P(•OH) formation from reaction (6). Radically different profiles were obtained when 0.50 mM Fe^{2+} was added to the initial solution, attaining overall decolorization in about 30-35 min in EF with a Pt or TiO_2 NTs anode (i.e., in the dark) and PEF with a Pt anode under UV illumination. Fig. 7a reveals that the solution was decolorized very rapidly and at similar rate in these three processes. This can be explained by the fast oxidation by homogeneous •OH, largely produced via Fenton's reaction (3), which became the preponderant oxidizing species in all these EAOPs. From the rather analogous decolorization rate in EF and PEF, it can be deduced that the photolytic reaction (4) had very little influence on •OH generation. It should be noted that during all these experiments, the initial solution pH of 3.0 remained practically constant.

The kinetic analysis of the above absorbance decays yielded good linear profiles with $R^2 \geq 0.98$, which can be associated with a pseudo-first-order reaction, at least during the first stages, as shown in Fig. 7b. From these correlations, an apparent decolorization rate constant (k_{dec}) of $(2.2\pm0.1)\times10^{-3}$ min^{-1} in EO-H_2O_2 with Pt was determined, growing to $(4.9\pm0.2)\times10^{-3}$ min^{-1} in EO with Pt/stainless steel cell and $(5.1\pm0.2)\times10^{-3}$ min^{-1} in PEC. As expected, much greater k_{dec} values ranging between 0.063 and 0.072 min^{-1} were obtained in the EF and PEF treatments. This kinetics involves a constant and small generation of oxidants in each EAOP tested.

Next, the PEC/PEF treatment of analogous Indigo Carmine solutions using TiO_2 NTs as photoanode and an air-diffusion cathode was assessed. Fig. 8a depicts the rapid fading of the solution in this EAOP at j = 3 mA cm^{-2}, reaching total decolorization in about 35 min, a time equal to that required under EF and PEF conditions with a Pt anode (see Fig. 7a). From the excellent linear fitting obtained, which agrees with a pseudo-first-order kinetics as depicted in

the inset of Fig. 8a, a similar k_{dec} = (0.058±0.002) min^{-1} (R^2 = 0.996) was determined in PEC/PEF. Therefore, it can be deduced that in all these processes, the main oxidant is •OH originated from Fenton's reaction (3), with only a minor role for the heterogeneous oxidants generated at the corresponding anode surface. Fig. 8a also shows a slower decolorization when the PEC/PEF process was made at a lower j = 2 mA cm^{-2}. Overall color loss was achieved after a longer electrolysis time of 50 min, with a smaller k_{dec} = (0.048±0.002) min^{-1} (R^2 = 0.992). This is indicative of a lower production of homogeneous •OH, as expected from the smaller generation of H_2O_2 due to the deceleration of reaction (2) as j decreases [2].

Fig. 8b depicts the abatement of Indigo Carmine concentration for the above PEC/PEF trials. Total dye removal after 40 and 35 min was reached at 2 and 3 mA cm^{-2}, respectively, which are similar or slightly shorter times as compared to those needed for decolorization (see Fig. 8a). These concentration decays also agreed with a pseudo-first-order reaction kinetics, as shown in the inset of Fig. 8b, corroborating the generation of a constant and small amount of oxidizing agents, pre-eminently •OH from Fenton's reaction (3) and, to a lesser extent, P(•OH) and h^+_{VB} formed from reactions (5) and (6). From this analysis, an increasing apparent rate constant for dye removal (k_1) of (0.054±0.002) min^{-1} (R^2 = 0.990) at j = 2 mA cm^{-2} and (0.083±0.004) min^{-1} (R^2 = 0.993) at j = 3 mA cm^{-2} was determined. Note that these k_1-values were greater than the corresponding k_{dec} ones, suggesting the formation of small quantities of colored by-products that also absorb at λ_{max} = 611 nm and slow down the decolorization process.

3.5. Mineralization of Indigo Carmine solutions

The mineralization of the 0.260 mM Indigo Carmine (50 mg L^{-1} TOC) solutions by the EO-H_2O_2, EF and PEF processes with Pt anode and the PEC/PEF process with TiO_2 NTs as photoanode under the above conditions was monitored from their TOC abatement for 480 min.

As can be seen in Fig. 9a, the EO-H_2O_2 process with Pt at j = 3 mA cm^{-2} led to an insignificant TOC removal of 4.6% due to the low oxidation ability of Pt(•OH) and H_2O_2 originated from reactions (1) and (2), respectively. The addition of 0.50 mM Fe^{2+} in the dark promoted the generation of homogeneous •OH by Fenton's reaction (3) in EF with Pt, with the consequent faster destruction of intermediates until a final TOC reduction of 43.2% was attained. The process was strongly accelerated in PEF with Pt, reaching 81.5% of TOC decay, as result of the additional fast photodecomposition of UV photoactive products, like Fe(III)-carboxylate complexes [2,30]. Fig. 9a reveals that the comparable PEC/PEF process, i.e., upon replacement of Pt by TiO_2 NTs photoanode, was slightly more powerful and TOC was rapidly reduced by 79.8% in 300 min. This was due to the more efficient removal of organics thanks to the contribution of h^+_{VB} and P(•OH), which acted in concomitance with bulk •OH and UV photons. At longer time, TOC abatement was slowed down and only decayed by 84.6% in 480 min, as a result of the formation of very refractory oxidation products. When a lower j = 2 mA cm^{-2} was employed, the mineralization was strongly decelerated, as expected from the smaller production of oxidants up to 300 min. Then, the profile tended to become similar to that at j = 3 mA cm^{-2} because of the formation of an analogous amount of recalcitrant products that accounted for the residual TOC. These findings show that the PEC/PEF treatment with TiO_2 NTs photoanode is slightly superior to PEF with active Pt to mineralize acidic Indigo Carmine solutions.

The inorganic ions released from the 0.260 mM Indigo Carmine solution were identified and monitored during the PEC/PEF process at j = 3 mA cm^{-2}. The initial S (0.520 mM) was completely converted into SO_4^{2-} ion. On the other hand, Fig. 10a presents the evolution of the NH_4^+ ion, which reached a final content of about 0.520 mM that matched perfectly with the initial N content. Based on these findings, the following total mineralization reaction for the dianion form of Indigo Carmine, the existing species in solution, with a number of exchanged electrons of n = 64 can be envisaged:

401 $C_{16}H_8N_2O_8S_2^{2-} + 32H_2O \rightarrow 16CO_2 + 2NH_4^+ + 2SO_4^{2-} + 64H^+ + 64e^-$ (12)

402 The percentage of mineralization current efficiency (MCE) for each treatment performed
403 at current *I* (in A) and time *t* (in h) was then estimated as follows [2,11]:

404 $$\text{MCE} = \frac{n\,F\,V\Delta\text{TOC}}{4.32\text{x}10^7 m\,I\,t}100 \quad (13)$$

405 where △TOC is the abated solution TOC (in mg L^{-1}), 4.32×10^7 is a constant for units
406 conversion (= 3600 s h^{-1} × 12000 mg C mol^{-1}) and *m* denotes the number of carbon atoms in
407 the dye (= 16).

408 Fig. 9b reflects the change of MCE with time for the trials of Fig. 9a. According to Eq.
409 (13), the MCE values at a given j = 3 mA cm^{-2} could be enhanced by causing a higher △TOC,
410 i.e., as the oxidation power of the EAOP became higher. Hence, at any given time, the MCE
411 rose in the sequence EO-H_2O_2 << EF << PEF < PEC/PEF. In PEC/PEF, the most powerful
412 process, a maximum MCE of 131.4% was obtained after 240 min of electrolysis, finally
413 dropping to 78.7% by the loss of organic load with generation of more recalcitrant products
414 [1,5]. MCE values higher than 100% are due to the potent oxidation action of light irradiation,
415 not considered in Eq. (13). A similar profile can be observed for PEF, although with lower
416 MCE, whereas this value was strongly reduced in EF because of its much smaller oxidation
417 ability. Fig. 9b also highlights the lower efficiency at the beginning of the PEC/PEF process at
418 j = 2 mA cm^{-2}, but attaining a greater maximum MCE of 146.6% at 360 min, once the most
419 recalcitrant products were already formed. This means that this lower *j* value allows a more
420 cost-effective treatment of Indigo Carmine solutions at pH 3.0, which can be of interest if
421 processing time is not a limiting factor.

422 *3.6. Identification of oxidation by-products*

423 The primary oxidation products of Indigo Carmine formed during the PEC/PEF assays
424 were identified by reversed-phase HPLC. These chromatograms only displayed one additional

peak, related to the colorless isatin-5-sulfonic acid. Fig. 10b highlights that at j = 2 mA cm^{-2}, this compound was accumulated up to 0.34 mM after 30-35 min, to further disappear at 100 min. At j = 3 mA cm^{-2}, a slightly higher accumulation of 0.38 mM at 25 min can be observed, followed by a faster removal with disappearance at 80 min, in agreement with the greater amount of oxidants produced. Isatin-5-sulfonic acid is formed upon attack of $^{\bullet}OH$ and P($^{\bullet}OH$) on the dye, with cleavage of the carbon double bond between the two indole moieties. Its high concentration during the destruction of 0.260 mM of the dye indicates that it constitutes its main oxidation by-product. Note that this main intermediate has also been reported during the Indigo Carmine treatment by EO with active IrO_2-SnO_2-Sb_2O_3 [41] and non-active BDD [29] and EF and PEF with non-active Pt and active BDD [30] at high j. Other possible heteroaromatic products like indigo [30] have not been detected.

Subsequent cleavage of the indole group of isatin-5-sulfonic acid is expected to yield short-chain linear carboxylic acids [30,41]. This was confirmed by identifying such final products by ion-exclusion HPLC analysis during the PEC/PEF treatment at j = 3 mA cm^{-2}. Traces of oxalic and oxamic acids (< 0.001 mM), along with a concentration of formic acid that gradually increased up to 0.10 mM at 480 min (see Fig. 10c), were detected. All these acids form Fe(III) complexes [2,5]. The larger accumulation of formic acid is indicative of a large stability of the Fe(III)-formate complexes against $^{\bullet}OH$, P($^{\bullet}OH$) and UV photons. From these results, one can infer that the final electrolyzed solution contained 1.2 mg L^{-1} of TOC related to small carboxylic acids, only representing a 15.6% of its residual TOC (see Fig. 9a). This means that the most of the undetected final products were largely recalcitrant, being responsible for the incomplete mineralization of the Indigo Carmine solution.

4. Conclusions

448 TiO_2 nanotube arrays synthesized by Ti anodization can be used as photoanodes to promote
449 the generation of h^+_{VB} and P(•OH) under UV irradiation, showing greater ability than Pt to
450 degrade Indigo Carmine solutions at pH 3.0. This was confirmed from the quicker
451 decolorization achieved by PEC with TiO_2 NTs as compared to EO-H_2O_2 with Pt, as well as
452 the faster mineralization attained using the hybrid PEC/PEF with TiO_2 NTs as compared to PEF
453 with Pt. The photoanode was highly stable at $j \leq 3$ mA cm^{-2} and its surface became more
454 compact upon prolonged electrolyses. The electrochemical characterization allow confirming
455 the TiO_2 NTs photoactivity, which increased from $E_{an} \geq +0.20$ V. •OH formed from Fenton's
456 reaction was the main oxidant in EF, PEF and PEC/PEF. The absorbance and Indigo Carmine
457 decays in these processes always obeyed a similar pseudo-first-order kinetics, although with
458 $k_{dec} < k_1$ due to the generation of colored products that slow down the decolorization process.
459 The mineralization power of the EAOPs grew in the order: EO-H_2O_2 << EF < PEF < PEC/PEF.
460 An 84.6% TOC abatement, with a maximum MCE of 87.6%, was found for the most powerful
461 treatment: PEC/PEF with TiO_2 NTs as photoanode, at $j = 3$ mA cm^{-2}. A lower mineralization
462 rate but ending in a similar mineralization degree and attaining a greater MCE of 97.7%, was
463 obtained at $j = 2$ mA cm^{-2}. The initial S and N of the dye were completely converted to SO_4^{2-}
464 and NH_4^+ ions. Isatin-5-sulfonic acid and formic acid were formed as primary and final
465 products, respectively.

466 **Acknowledgements**

467 This work was mainly conducted within the framework of a collaborative program between
468 the University of São Paulo and the Universitat de Barcelona under Grant AUCANI no. 787.
469 Financial support from project CTQ2016-78616-R (AEI/FEDER, EU) and the PhD fellowship
470 awarded to R. Oriol by MINECO (Spain) are acknowledged. A. R. De Andrade also
471 acknowledges the funding provided by Brazilian agencies including the Brazilian National

Council for Scientific and Technological Development - CNPq (grant no. 465571/2014-0), São Paulo Research Foundation (FAPESP grant 50945-4) and the Coordenação de Aperfeiçoamento de Pessoal de Nível Superior Brasil (CAPES) Finance Code 001.

References

[1] M. Panizza, G. Cerisola, Direct and mediated anodic oxidation of organic pollutants, Chem. Rev. 109 (2009) 6541–6569.

[2] E. Brillas, I. Sirés, M.A. Oturan, Electro-Fenton process and related electrochemical technologies based on Fenton's reaction chemistry, Chem. Rev. 109 (2009) 6570–6631.

[3] S. Vasudevan, M.A. Oturan, Electrochemistry: as cause and cure in water pollution-an overview, Environ. Chem. Lett. 12 (2014) 97–108.

[4] L. Feng, E.D. van Hullebusch, M.A. Rodrigo, G. Esposito, M.A. Oturan, Removal of residual anti-inflammatory and analgesic pharmaceuticals from aqueous systems by electrochemical advanced oxidation processes. A review, Chem. Eng. J. 228 (2013) 944–964.

[5] C.A. Martínez-Huitle, M.A. Rodrigo, I. Sirés, O. Scialdone, Single and coupled electrochemical processes and reactors for the abatement of organic water pollutants: a critical review, Chem. Rev. 115 (2015) 13362–13407.

[6] B. Boye, P.A. Michaud, B. Marselli, M.M. Dieng, E. Brillas, C. Comninellis, Anodic oxidation of 4-chlorophenoxyacetic acid on synthetic boron-doped diamond electrodes, New Diamond Frontier Carbon Technol. 12 (2002) 63–72.

[7] M.A. Oturan, I. Sirés, N. Oturan, S. Pérocheau, J.-L. Laborde, S. Trévin, Sonoelectro-Fenton process: A novel hybrid technique for the destruction of organic pollutants in water, J. Electroanal. Chem. 624 (2008) 329–332.

[8] A. El-Ghenymy, R.M. Rodríguez, E. Brillas, N. Oturan, M.A. Oturan, Electro-Fenton degradation of the antibiotic sulfanilamide with Pt/carbon-felt and BDD/carbon-felt cells. Kinetics, reaction intermediates, and toxicity assessment, Environ. Sci. Pollut. Res. 21 (2014) 8368–8378.

[9] O. Ganzenko, N. Oturan, I. Sirés, D. Huguenot, E.D. van Hullebusch, G. Esposito, M.A. Oturan, Fast and complete removal of the 5-fluorouracil drug from water by electro-Fenton oxidation, Environ. Chem. Lett. 16 (2018) 281–286.

[10] A. Galia, S. Lanzalaco, M.A. Sabatino, C. Dispenza, O. Scialdone, I. Sirés, Crosslinking of poly(vinylpyrrolidone) activated by electrogenerated hydroxyl radicals: A first step towards a simple and cheap synthetic route of nanogel vectors, Electrochem. Commun. 62 (2016) 64-68.

[11] J.R. Steter, E. Brillas, I. Sirés, On the selection of the anode material for the electrochemical removal of methylparaben from different aqueous media, Electrochim. Acta 222 (2016) 1464–1474.

[12] S. Lanzalaco, I. Sirés, M.A. Sabatino, C. Dispenza, O. Scialdone, A. Galia, Synthesis of polymer nanogels by electro-Fenton process: investigation of the effect of main operation parameters, Electrochim. Acta 246 (2017) 812–822.

[13] J.R. Steter, E. Brillas, I. Sirés, Solar photoelectro-Fenton treatment of a mixture of parabens spiked into secondary treated wastewater effluent at low input current, Appl. Catal. B: Environ. 224 (2018) 410–418.

[14] S. Lanzalaco, I. Sirés, A. Galia, M.A. Sabatino, C. Dispenza, O. Scialdone, Facile crosslinking of poly(vinylpyrrolidone) by electro-oxidation with IrO_2-based anode under potentiostatic conditions, J. Appl. Electrochem. 48 (2018) 1343–1352.

518 [15] M.-Z. Ge, C.-Y. Cao, J.-Y. Huang, S.-H. Li, S.-N. Zhang, S. Deng, Q.-S. Li, K.-Q. Zhang,
519 Y.-K. Lai, Synthesis, modification, and photo/photoelectrocatalytic degradation
520 applications TiO_2 nanotube arrays: a review, Nanotechnol. Rev. 5 (2016) 75–112.
521 [16] S. Garcia-Segura, E. Brillas, Applied photoelectrocatalysis on the degradation of organic
522 pollutants in wastewaters, J. Photochem. Photobiol. C: Photochem. Rev. 31 (2017) 1–35.
523 [17] G. Ramírez, F.J. Recio, P. Herrasti, C. Ponce-de-León, I. Sirés, Effect of RVC porosity
524 on the performance of PbO_2 composite coatings with titanate nanotubes for the
525 electrochemical oxidation of azo dyes, Electrochim. Acta (2016) 9–17.
526 [18] G.G. Bessegato, F.F. Hudari, M.V.B. Zanoni, Self-doped TiO_2 nanotube electrodes: A
527 powerful tool as a sensor platform for electroanalytical applications, Electrochim. Acta
528 235 (2017) 527–533.
529 [19] L.C. Almeida, B.F. Silva, M.V.B. Zanoni, Combined photoelectrocatalytic/electro-
530 Fenton process using a Pt/TiO_2NTs photoanode for enhanced degradation of an azo dye:
531 A mechanistic study, J. Electroanal. Chem. 734 (2014) 43–52.
532 [20] K. Esquivel, L.G. Arriaga, F.J. Rodríguez, L. Martínez, L.A. Godínez, Development of a
533 TiO_2 modified optical fiber electrode and its incorporation into a photoelectrochemical
534 reactor for wastewater treatment, Water Res. 43 (2009) 3593–3603.
535 [21] R. Hernández, I. Olvera-Rodriguez, C. Guzmán, A. Medel, L. Escobar-Alarcón, E.
536 Brillas, I. Sirés, K. Esquivel, Microwave-assisted sol-gel synthesis of an Au-TiO_2
537 photoanode for the advanced oxidation of paracetamol as model pharmaceutical
538 pollutant, Electrochem. Commun. 96 (2018) 42–46.
539 [22] A.R. Khataee, M. Safarpour, M. Zarei, S. Aber, Combined heterogeneous and
540 homogeneous photodegradation of a dye using immobilized TiO_2 nanophotocatalyst and
541 modified graphite electrode with carbon nanotubes, J. Mol. Catal. A: Chem. 363–364
542 (2012) 58–68.

543 [23] L.C. Almeida, B.F. Silva, M.V.B. Zanoni, Photoelectrocatalytic/photoelectro-Fenton
544 coupling system using a nanostructured photoanode for the oxidation of a textile dye:
545 kinetics study and oxidation pathway, Chemosphere 136 (2015) 63–71.
546 [24] E. Mousset, V. Huang Weiqi, B. Foong Yang Kai, J.S. Koh, J.W. Tng, Z. Wang, O.
547 Lefebvre, A new 3D-printed photoelectrocatalytic reactor combining the benefits of a
548 transparent electrode and the Fenton reaction for advanced wastewater treatment, J.
549 Mater. Chem. A 5 (2017) 24951–24964.
550 [25] Q. Zhou, A. Xing, J. Li, D. Zhao, K. Zhao, M. Lei, Synergistic enhancement in
551 photoelectrolytic degradation of bisphenol A by CeO_2 and reduced graphene oxide co-
552 modified TiO_2 nanotube arrays in combination with Fenton oxidation, Electrochim. Acta
553 209 (2016) 379–388.
554 [26] Z. Peng, Z. Yu, L. Wang, Y. Liu, G. Xiang, Y. Chen, L. Sun, J. Huang, Synthesis of
555 Fe_2O_3/TiO_2 nanotube and its application in photoelectrocatalytic/photoelectro-Fenton
556 decolorization of rhodamine B, J. Adv. Oxid. Technol. 19 (2016) 34–42.
557 [27] A.R. Khataee, M. Zarei, Photoelectrocatalytic decolorization of diazo dye by zinc oxide
558 nanophotocatalyst and carbon nanotube based cathode: determination of the degradation
559 products, Desalination 278 (2011) 117–125.
560 [28] Y. Li, H. Li, M. Li, C. Li, Y. Lei, D. Sun, B. Yang, Fabrication and catalytic activities of
561 anodes consisting of ZnO nanorods on boron-doped diamond film, J. Alloys Compd. 743
562 (2018) 187–195.
563 [29] S. Ammar, R. Abdelhedi, C. Flox, C. Arias, E. Brillas, Electrochemical degradation of
564 the dye indigo carmine at boron-doped diamond anode for wastewaters remediation,
565 Environ. Chem. Lett. 4 (2006) 229–233.

566 [30] C. Flox, S. Ammar, C. Arias, E. Brillas, A.V. Vargas-Zavala, R. Abdelhedi, Electro-
567 Fenton and photoelectro-Fenton degradation of indigo carmine in acidic aqueous
568 medium, Appl. Catal. B: Environ. 67 (2006) 93–104.
569 [31] P.C. Genazio Pereira, R.V. Reimao, T. Pavesi, E.M. Saggioro, J.C. Moreira, F. Verissimo
570 Correia, Lethal and sub-lethal evaluation of indigo carmine and byproducts after TiO_2
571 photocatalysis in the immune system of *Eisenia andrei* earthworms, Ecotox. Environ.
572 Safe. 143 (2017) 275–282.
573 [32] E.M. Saggioro, A.S. Oliveira, T. Pavesi, M.J. Tototzintle, M.I. Maldonado, F.V. Correia,
574 J.C. Moreira, Solar CPC pilot plant photocatalytic degradation of indigo carmine dye in
575 waters and wastewaters using supported-TiO_2: influence of photodegradation parameters,
576 Int. J. Photoenergy (2015) 656153.
577 [33] Y.V. Marathe, V.S. Shrivastava, Degradation of indigo carmine dye by sol gel deposited
578 nanocrystaline cadmium sulphide thin film, Adv. Sci. Lett. 5 (2012) 173–177.
579 [34] D.J. Kim, W.-K. Jo, Sustainable treatment of harmful dyeing industry pollutants using
580 $SrZnTiO_3$/g-C_3N_4 heterostructure with a light source-dependent charge transfer
581 mechanism, Appl. Catal. B: Environ. 242 (2019) 171–177.
582 [35] T.T. Guaraldo, S.H. Pulcinelli, M.V.B. Zanoni, Influence of particle size on the
583 photoactivity of Ti/TiO_2 thin film electrodes, and enhanced photoelectrocatalytic
584 degradation of indigo carmine dye, J. Photochem. Photobiol. A: Chem. 217 (2011) 259–
585 266.
586 [36] T.T. Guaraldo, T.B. Zanoni, S.I.C. de Torresi, V.R. Goncales, G.J. Zocolo, D.P. Oliveira,
587 M.V.B. Zanoni, On the application of nanostructured electrodes prepared by
588 Ti/TiO_2/WO_3 "template": A case study of removing toxicity of indigo using visible
589 irradiation, Chemosphere 91 (2013) 586–593.

590 [37] P. Acevedo-Peña, J.E. Carrera-Crespo, F. González, I. González, Effect of heat treatment
591 on the crystal phase composition, semiconducting properties and photoelectrocatalytic
592 color removal efficiency of TiO_2 nanotubes arrays, Electrochim. Acta 140 (2014) 564–
593 571.
594 [38] M. Ureña de Vivanco, M. Rajab, C. Heim, T. Letzel, B. Helmreich, Setup and energetic
595 considerations for three advanced oxidation reactors treating organic compounds, Chem.
596 Eng. Technol. 36 (2013) 355–361.
597 [39] R.E. Palma-Goyes, J. Silva-Agredo, I. González, R.A. Torres-Palma, Comparative
598 degradation of indigo carmine by electrochemical oxidation and advanced oxidation
599 processes, Electrochim. Acta 140 (2014) 427–433.
600 [40] L. Labiadh, A. Barbucci, M.P. Carpanese, A. Gadri, S. Ammar, M. Panizza, Direct and
601 indirect electrochemical oxidation of indigo carmine using PbO_2 and $TiRuSnO_2$, J. Solid
602 State Electrochem. 21 (2017) 2167–2175.
603 [41] R.E. Palma-Goyes, J. Silva-Agredo, J. Vázquez-Arenas, I. Romero-Ibarra, R.A. Torres-
604 Palma, The effect of different operational parameters on the electrooxidation of indigo
605 carmine on Ti/IrO_2-SnO_2-Sb_2O_3, J. Environ. Chem. Eng. 6 (2018) 3010–3017.
606 [42] D. Stergiopoulos, K. Dermentzis, P. Giannakoudakis, S. Sotiropoulos, Electrochemical
607 decolorization and removal of indigo carmine textile dye from wastewater, Global NEST
608 J. 16 (Spec. Iss. 3) (2014) 501–508.
609 [43] Sowbhagy, S. Ananda, Rakesh, Electrochemical degradation of indigo carmine dye at
610 Ru-doped platinum anode in aqueous solution, Int. J Appl. Chem. 8 (2012) 141–152.
611 [44] L.C. Almeida, S. Garcia-Segura, C. Arias, N. Bocchi, E. Brillas, Electrochemical
612 mineralization of the azo dye Acid Red 29 (Chromotrope 2R) by photoelectro-Fenton
613 process, Chemosphere 89 (2012) 751–758.

[45] F.J. Welcher, Standard Methods of Chemical Analysis, 6th Ed., Vol. 2, part B, R.E. Krieger Publishing Co, Huntington, New York, 1975.

[46] E. Bocos, E. Brillas, M.A. Sanromán, I. Sirés, Electrocoagulation: Simply a phase separation technology? The case of bronopol compared to its treatment by EAOPs, Environ. Sci. Technol. 50 (2016) 7679–7686.

[47] H. Pelouchova, P. Janda, J. Weber, L. Kavan, Charge transfer reductive doping of single crystal TiO_2 anatase, J. Electroanal. Chem. 566 (2004) 73–83.

622 **Figure captions**

623 **Fig. 1.** Molecular structure of (a) Indigo Carmine, (b) indigo and (c) isatin-5-sulfonic acid.

624 **Fig. 2.** Sketch of the electrolytic cell used for the PEC/PEF treatment of Indigo Carmine
625 solutions, equipped with a TiO_2 NTs photoanode and an air-diffusion cathode upon irradiation
626 with a 36-W UV LED lamp.

627 **Fig. 3.** Selected FE-SEM images of TiO_2 NTs grown by Ti anodization, at different
628 magnifications. View of: (a) a fresh electrode and (b) the electrode used as photoanode in all
629 the hybrid photoelectrocatalysis (PEC)/photoelectro-Fenton (PEF) trials at current density (*j*)
630 of 2-3 mA cm^{-2}. Pristine electrodes showing a selection of (c) inner and (d) outer diameters of
631 the nanotubes. Cross-section of a pristine electrode showing (e) the thickness of the Ti substrate
632 and (f) the estimated length of the nanotubes.

633 **Fig. 4.** EDX spectra of: (a) pristine TiO_2 NTs and (b) photoanode used in all the PEC/PEF
634 experiments made at 2-3 mA cm^{-2}.

635 **Fig. 5.** (a) Cyclic voltammograms recorded for the synthesized TiO_2 NTs (1 cm^2) photoanode
636 in 80 mL of 0.050 M Na_2SO_4 solution at pH 3.0 and 25 ºC (- - -) in the dark and (——) under
637 illumination with a 36-W UV LED lamp. Counter electrode: Pt sheet; reference electrode: SCE.
638 Initial and final potential: -2.00 V; reversal potential: +3.00 V. Scan rate: 10 mV s^{-1}. (b)
639 Consecutive chronoamperograms obtained using the same system, but with 0.100 M Na_2SO_4
640 solution at pH 3.0, operating in the dark for 60 s (i.e., switched off lamp) and under irradiation
641 with the 36-W UV LED lamp for 60 s (switched on lamp). Applied anodic potential: +0.20 V.

642 **Fig. 6.** Change of (a) accumulated H_2O_2 concentration and (b) its current efficiency with
643 electrolysis time using 150 mL of a 0.050 M Na_2SO_4 solution with 0.50 mM Fe^{2+}, at pH 3.0
644 and 25 ºC, using a 3 cm^2 (■) Pt anode (PEF conditions) or (●) TiO_2 NTs photoanode (PEC/PEF
645 conditions), combined with a 3 cm^2 air-diffusion cathode and under irradiation with a 36-W

UV LED lamp, operating at j = 3 mA cm^{-2}.

Fig. 7. (a) Percentage of color removal and (b) pseudo-first-order kinetic analysis for absorbance decay vs. electrolysis time for the degradation of 150 mL of a 0.260 mM Indigo Carmine solution with 0.050 M Na_2SO_4 at pH 3.0, 25 ºC and j = 3 mA cm^{-2}. (△) Electrochemical oxidation (EO) with a Pt/stainless steel cell. The other trials were made using an air-diffusion cathode: (□) EO with electrogenerated H_2O_2 (EO-H_2O_2) using a Pt anode, (○) PEC with TiO_2 NTs as photoanode under irradiation with a 36-W UV LED lamp, electro-Fenton (EF) with 0.50 mM Fe^{2+} and a (▲) Pt or (◆) TiO_2 NTs anode, and (■) PEF with 0.50 mM Fe^{2+} and a Pt anode under UV irradiation.

Fig. 8. Variation of (a) percentage of color removal and (b) Indigo Carmine concentration with electrolysis time for the PEC/PEF degradation of 150 mL of a 0.260 mM dye solution with 0.050 M Na_2SO_4 and 0.50 mM Fe^{2+} at pH 3.0 and 25 ºC using TiO_2 NTs as photoanode under irradiation with a 36-W UV LED lamp. Applied j: (▼) 2 mA cm^{-2} and (●) 3 mA cm^{-2}. The insets of plot (a) and (b) present the pseudo-first-order kinetic analysis for absorbance and concentration decays, respectively.

Fig. 9. Change of (a) TOC and (b) mineralization current efficiency with electrolysis time for the treatment of 150 mL of a 0.260 mM dye solution with 0.050 M Na_2SO_4 at pH 3.0 and 25 ºC using an air-diffusion cathode. (□) EO-H_2O_2 with a Pt anode, (▲) EF with a Pt anode and 0.50 mM Fe^{2+}, (■) PEF with a Pt anode and 0.50 mM Fe^{2+}, and (▼,●) PEC/PEF with TiO_2 NTs as photoanode and 0.50 mM Fe^{2+}. In the two latter methods, the solution was irradiated with a 36-W UV LED lamp. Applied j: (▼) 2 mA cm^{-2} and (□,▲,■,●) 3 mA cm^{-2}.

Fig. 10. Evolution of (a) NH_4^+, (b) isatin-5-sulfonic acid and (c) formic acid concentrations during the PEC/PEF treatment of 150 mL of a 0.260 mM Indigo Carmine solution with 0.050 M Na_2SO_4 and 0.50 mM Fe^{2+} at pH 3.0 and 25 ºC using TiO_2 NTs as photoanode and an air-diffusion cathode. Applied j: (▼) 2 mA cm^{-2} and (●) 3 mA cm^{-2}.

a

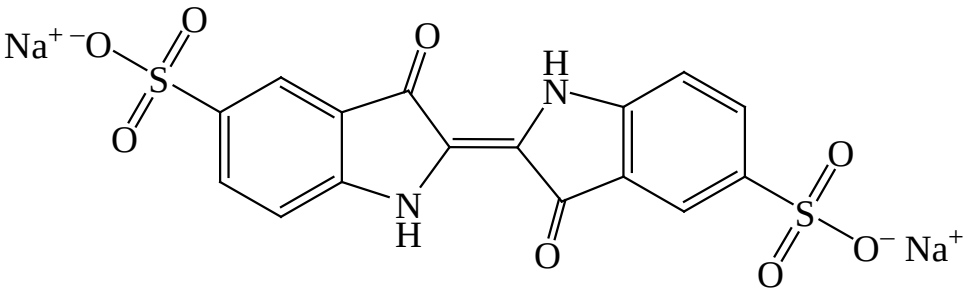

b

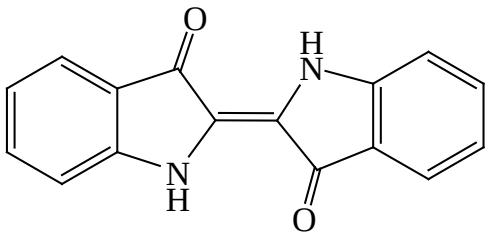

c

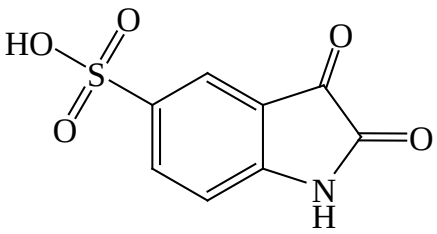

Fig. 1

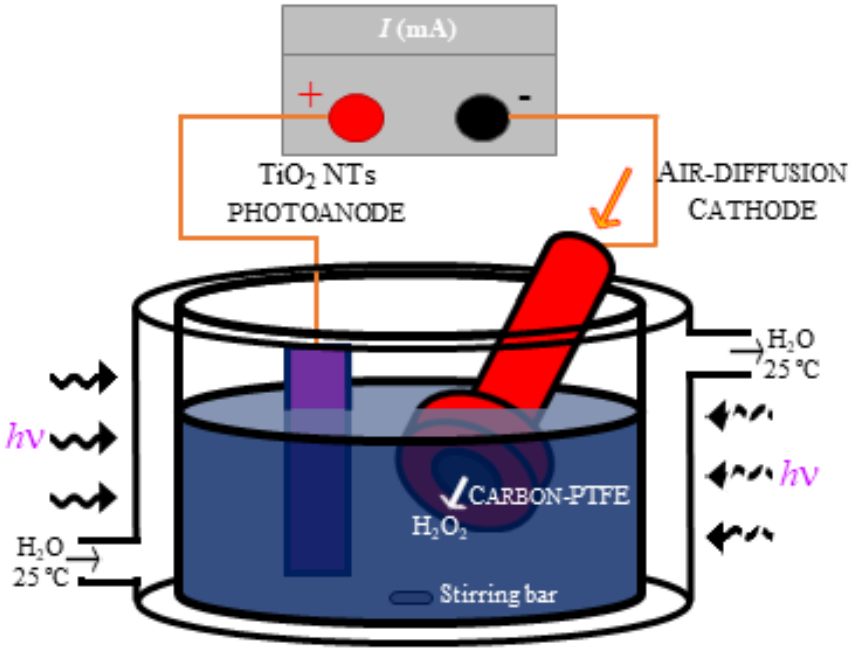
I (mA)
+
-
TiO2 NTs
PHOTOANODE
AIR-DIFFUSION
CATHODE
H2O
25 °C
hν
hν
CARBON-PTFE
H2O2
H2O
25 °C
Stirring bar

Fig. 2

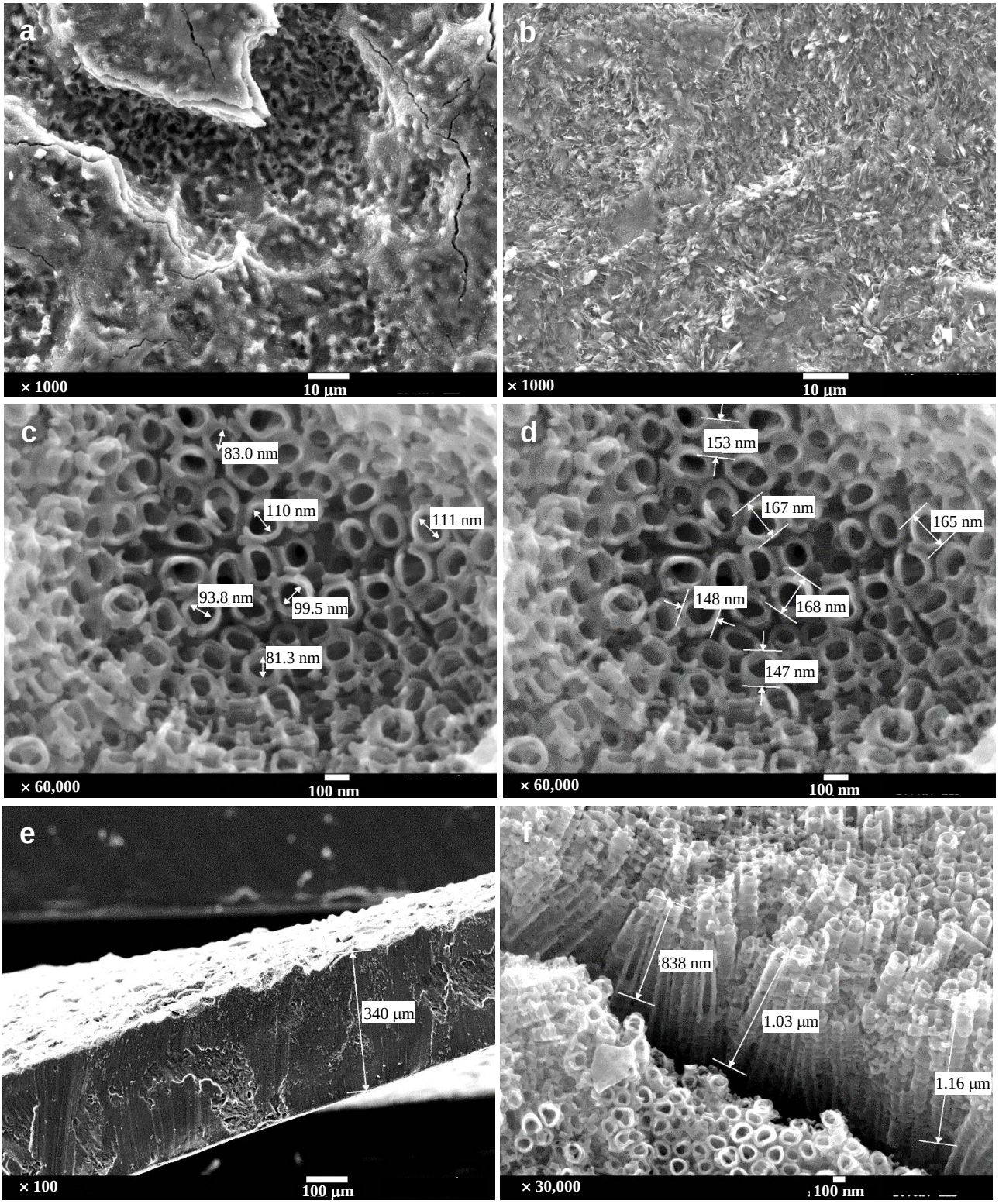
a
× 1000
10 µm
b
× 1000
10 µm
c
83.0 nm
110 nm
111 nm
93.8 nm
99.5 nm
81.3 nm
× 60,000
100 nm
d
153 nm
167 nm
165 nm
148 nm
168 nm
147 nm
× 60,000
100 nm
e
340 µm
× 100
100 µm
f
838 nm
1.03 µm
1.16 µm
× 30,000
100 nm

Fig. 3

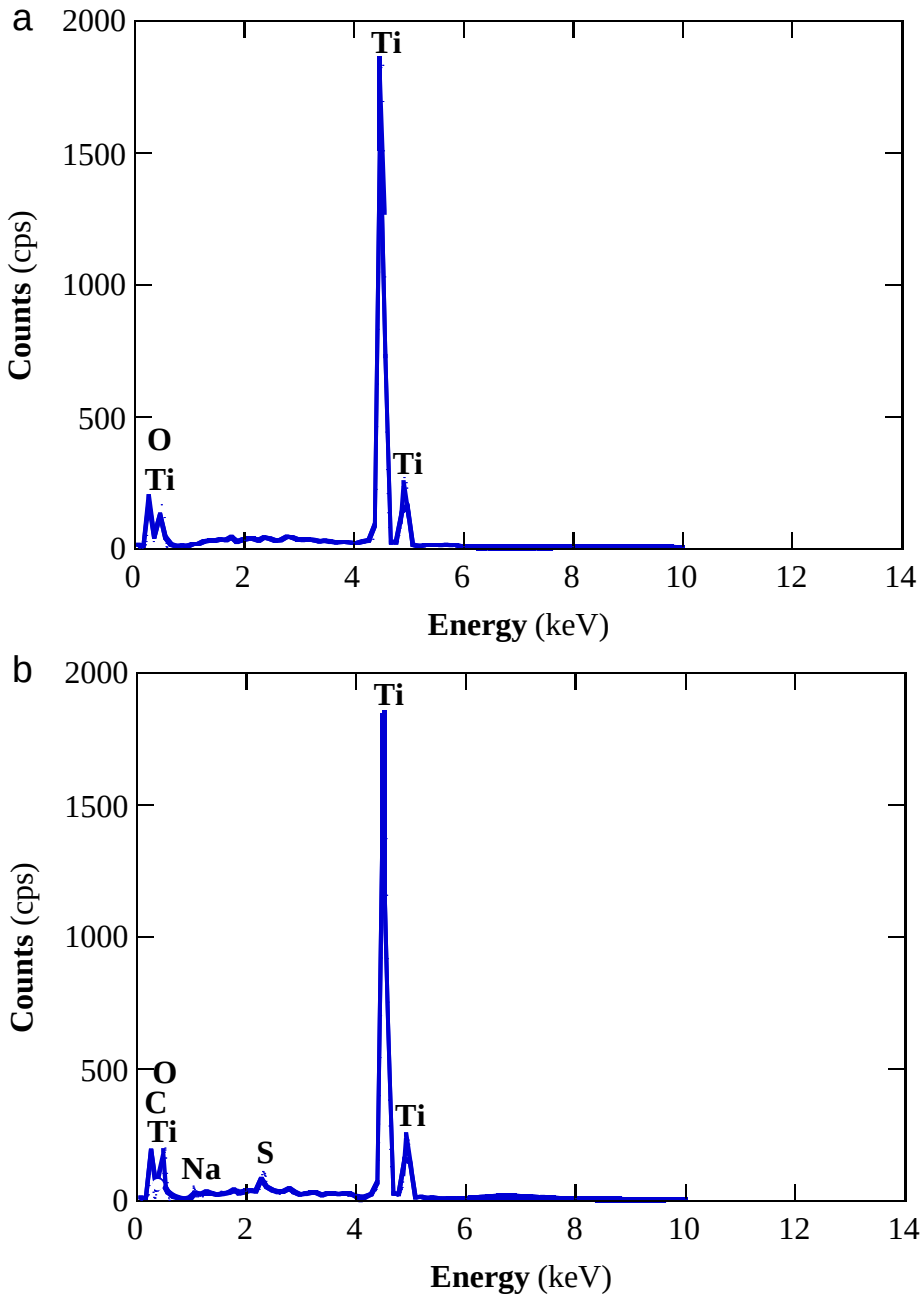
a
2000
1500
1000
500
0
Counts (cps)
Ti
O
Ti
Ti
0
2
4
6
8
10
12
14
Energy (keV)
b
2000
1500
1000
500
0
Counts (cps)
Ti
O
C
Ti
Na
S
Ti
0
2
4
6
8
10
12
14
Energy (keV)

Fig. 4

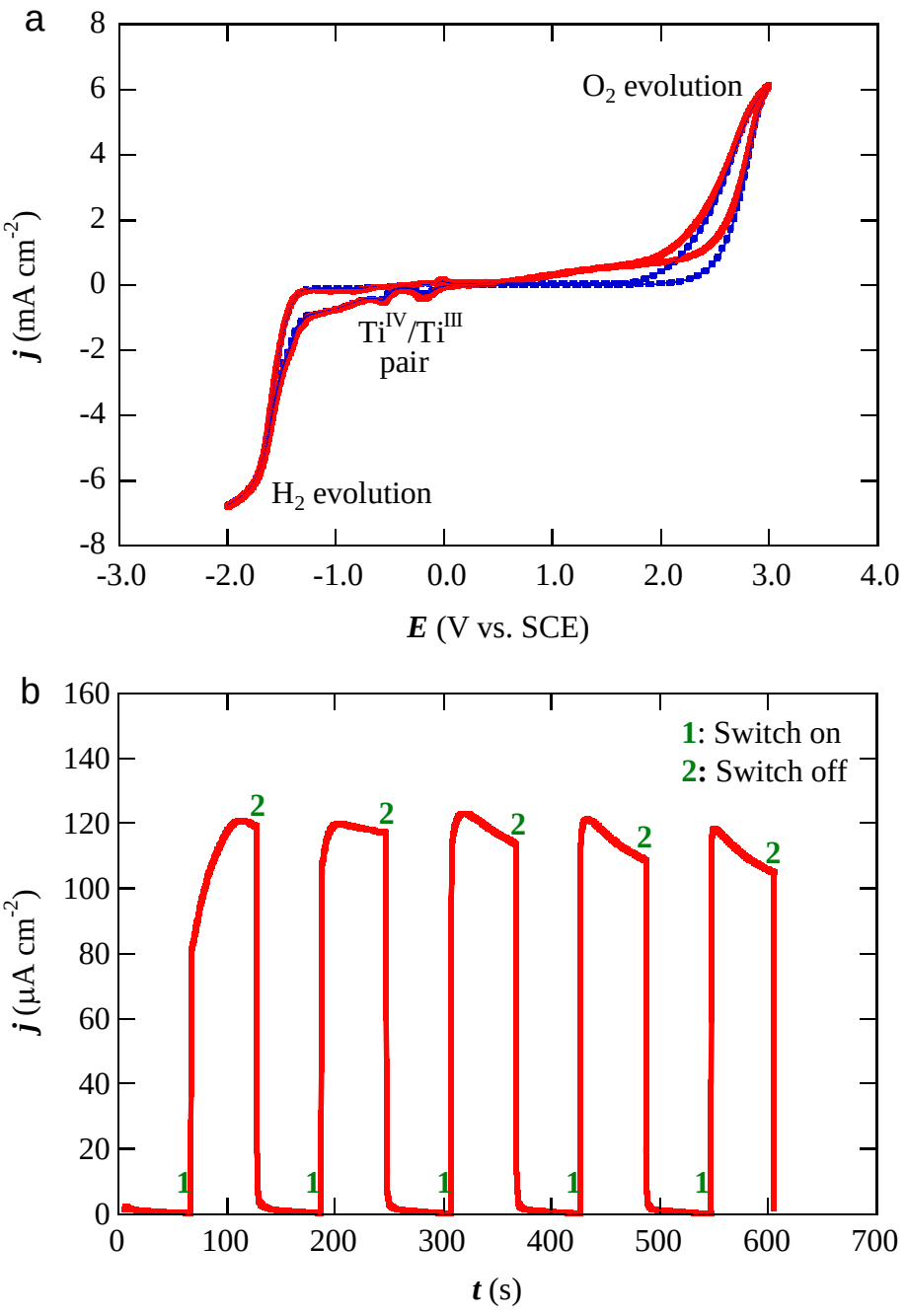
a
8
6
4
2
0
-2
-4
-6
-8
-3.0
-2.0
-1.0
0.0
1.0
2.0
3.0
4.0
O2 evolution
TiIV/TiIII
pair
H2 evolution
j (mA cm-2)
E (V vs. SCE)
b
160
140
120
100
80
60
40
20
0
0
100
200
300
400
500
600
700
1: Switch on
2: Switch off
1
2
j (μA cm-2)
t (s)

Fig. 5

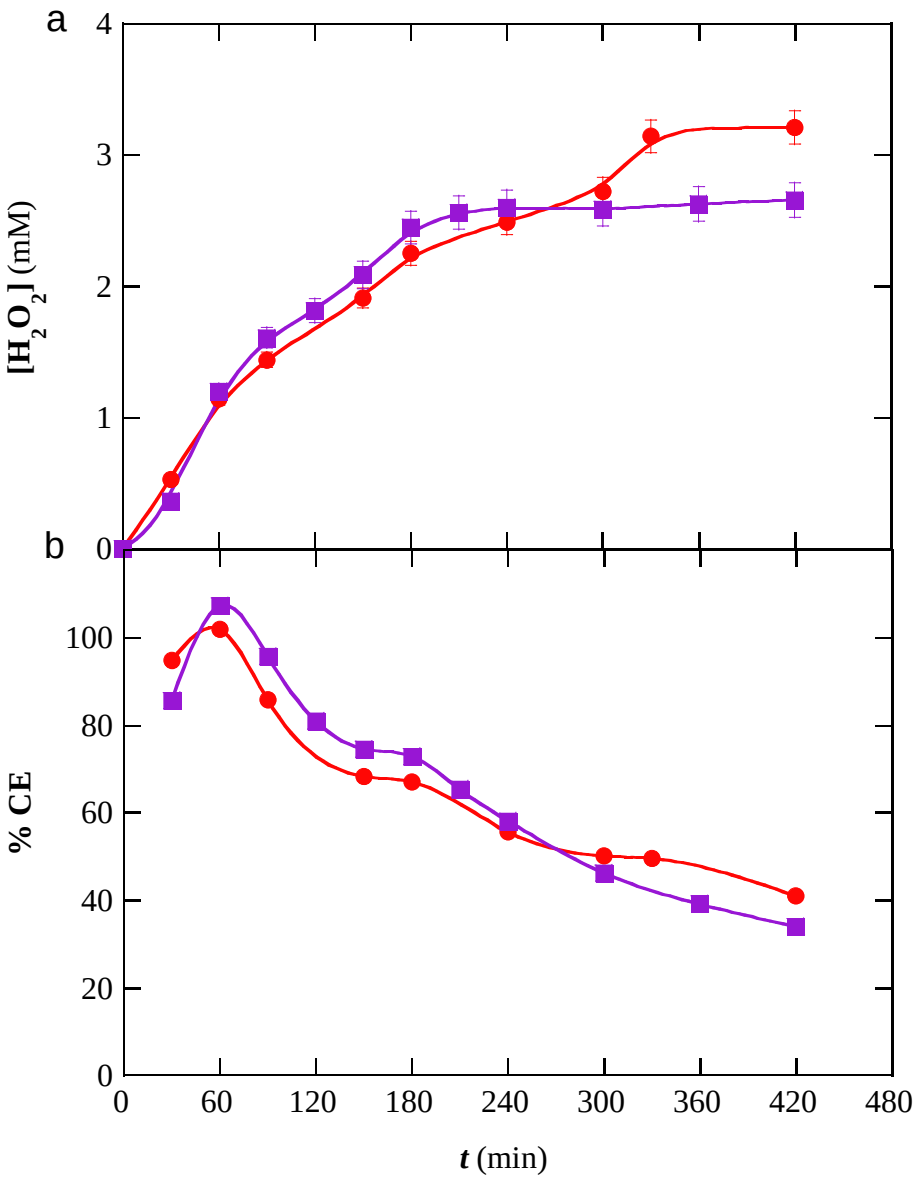
a
b
[H2O2] (mM)
% CE
t (min)
0
1
2
3
4
20
40
60
80
100
0
60
120
180
240
300
360
420
480

Fig. 6

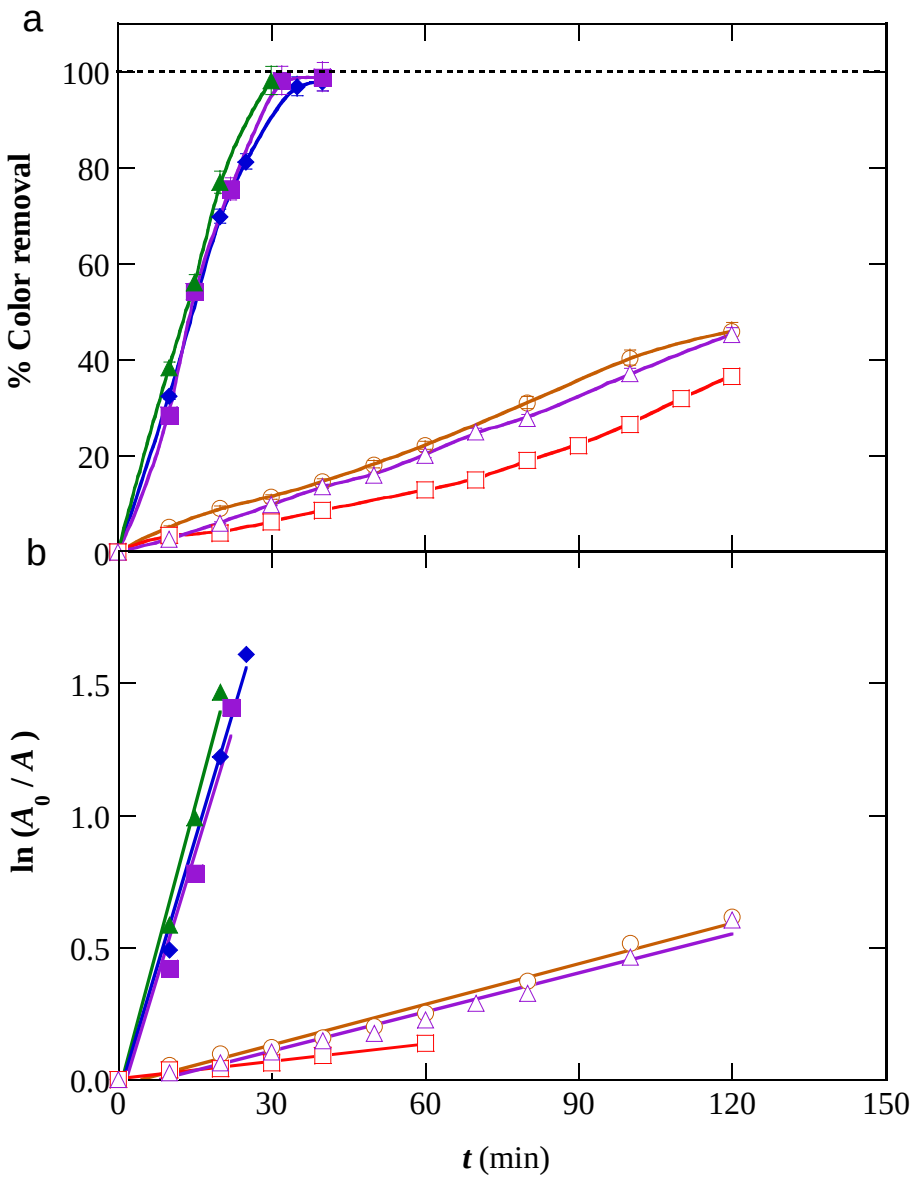
a
b
% Color removal
ln (A_0 / A)
t (min)
0
20
40
60
80
100
0.0
0.5
1.0
1.5
0
30
60
90
120
150

Fig. 7

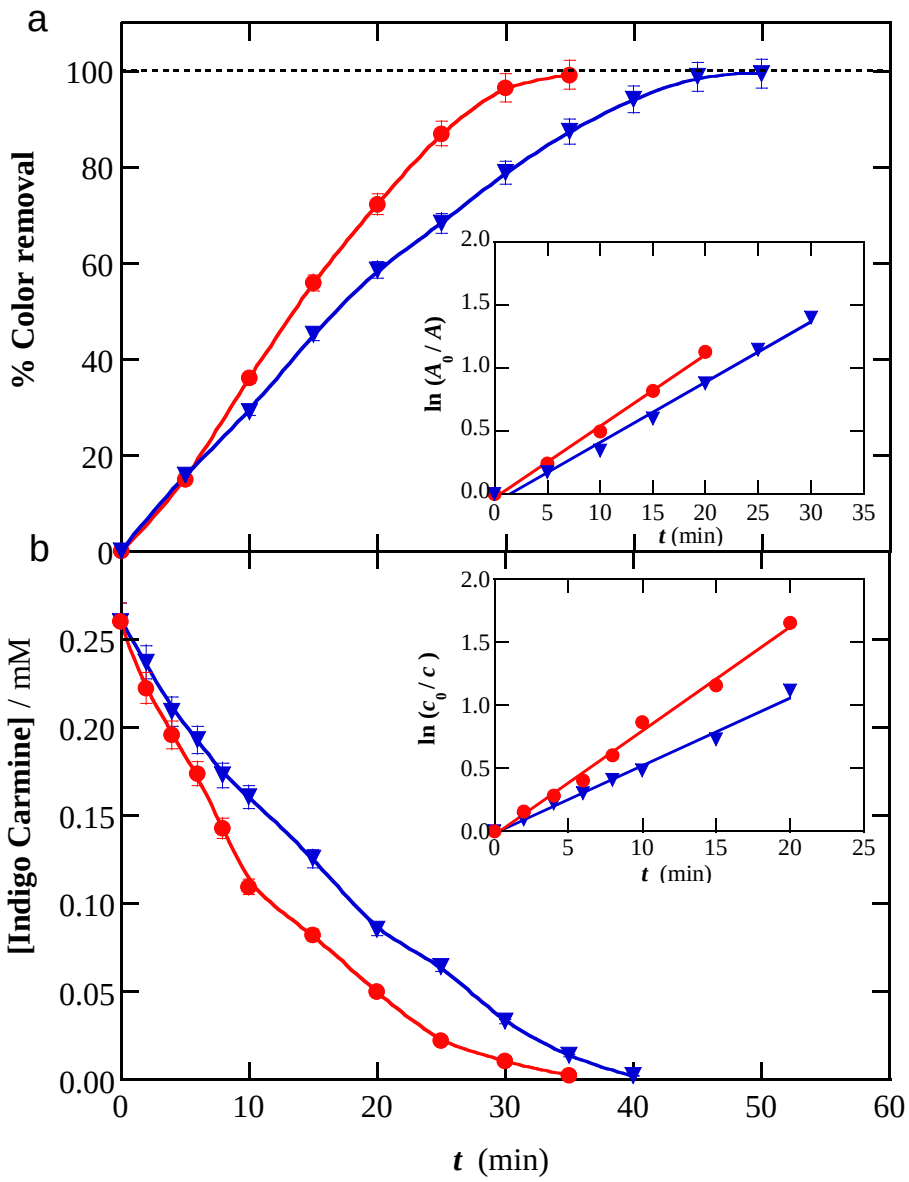
a
% Color removal
100
80
60
40
20
0
ln (A0 / A)
2.0
1.5
1.0
0.5
0.0
0
5
10
15
20
25
30
35
t (min)
b
[Indigo Carmine] / mM
0.25
0.20
0.15
0.10
0.05
0.00
ln (c0 / c)
2.0
1.5
1.0
0.5
0.0
0
5
10
15
20
25
t (min)
0
10
20
30
40
50
60
t (min)

Fig. 8

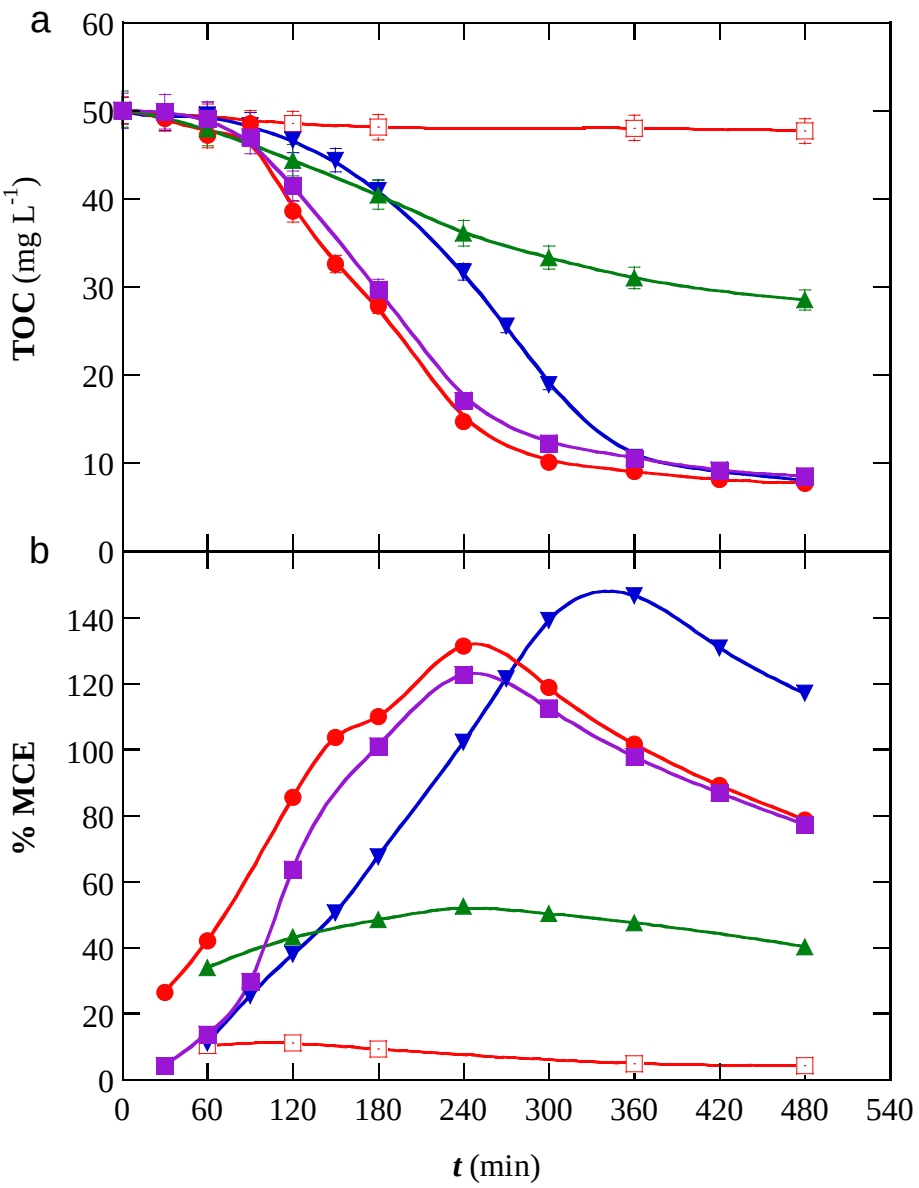
a
b
TOC (mg L-1)
% MCE
t (min)
0
10
20
30
40
50
60
0
20
40
60
80
100
120
140
0
60
120
180
240
300
360
420
480
540

Fig. 9

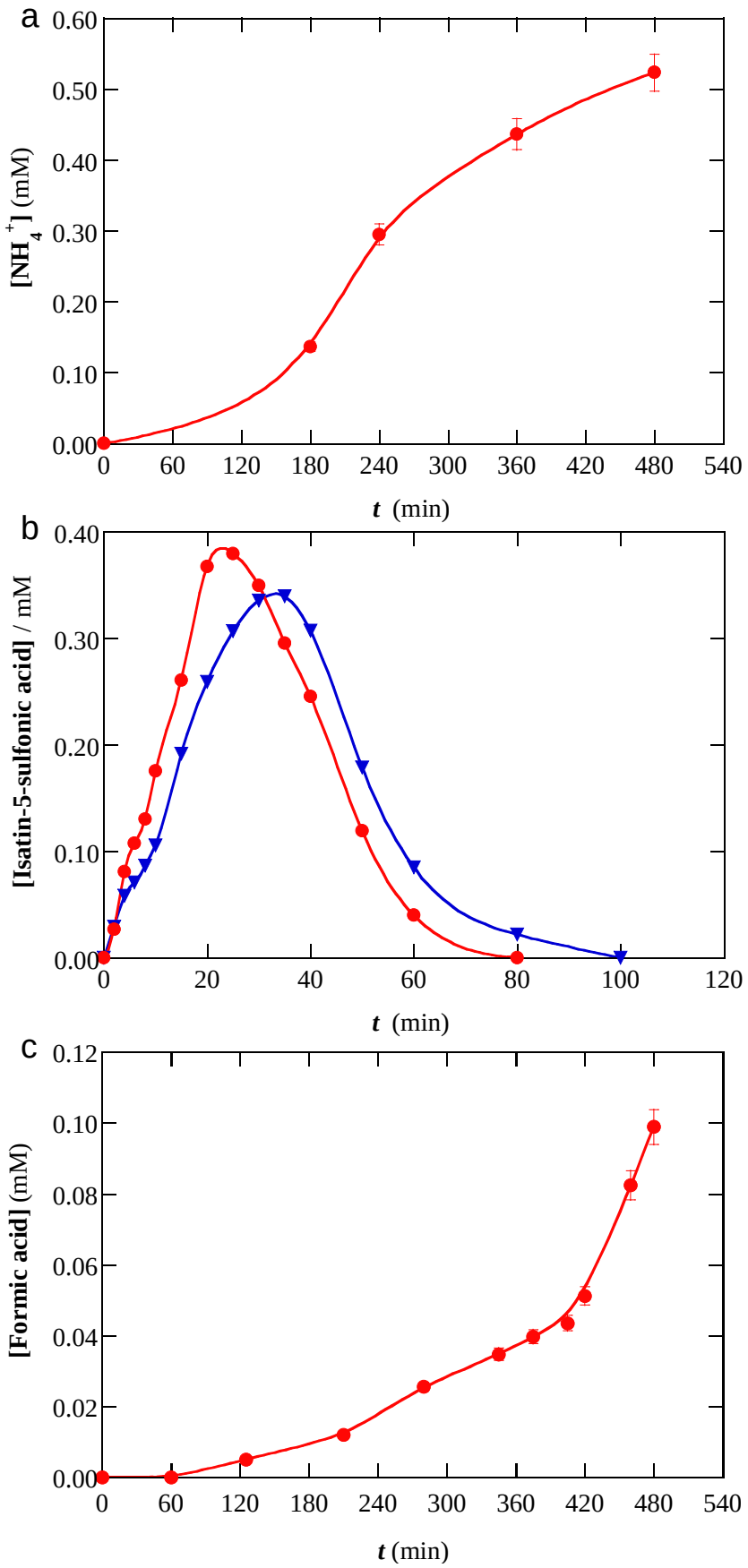
a
0.60
0.50
0.40
0.30
0.20
0.10
0.00
[NH4+] (mM)
0
60
120
180
240
300
360
420
480
540
t (min)
b
0.40
0.30
0.20
0.10
0.00
[Isatin-5-sulfonic acid] / mM
0
20
40
60
80
100
120
t (min)
c
0.12
0.10
0.08
0.06
0.04
0.02
0.00
[Formic acid] (mM)
0
60
120
180
240
300
360
420
480
540
t (min)

Fig. 10